2015

Continuous third harmonic generation in a terahertz driven modulated nanowire

Kathleen E. Hamilton
University of California - Riverside, kathleen.hamilton@email.ucr.edu

Alexey Kovalev
University of Nebraska-Lincoln, alexey.kovalev@unl.edu

Amrit De
University of California - Riverside, amritde@gmail.com

Leonid P. Pryadko
University of California - Riverside, leonid@ucr.edu

JOURNAL OF APPLIED PHYSICS 117, 213103 (2015)

Continuous third harmonic generation in a terahertz driven modulated nanowire

Kathleen E. Hamilton,[1,a)] Alexey A. Kovalev,[2] Amrit De,[1] and Leonid P. Pryadko[1]
[1]Department of Physics and Astronomy, University of California, Riverside, California 92521, USA
[2]Department of Physics and Astronomy and Nebraska Center for Materials and Nanoscience, University of Nebraska, Lincoln, Nebraska 68588, USA

(Received 30 September 2014; accepted 20 May 2015; published online 1 June 2015)

We consider the possibility of observing continuous third-harmonic generation using a strongly driven, single-band one-dimensional metal. In the absence of scattering, the quantum efficiency of frequency tripling for such a system can be as high as 93%. Combining the Floquet quasi-energy spectrum with the Keldysh Green's function technique, we derive a semiclassical master equation for a one-dimensional band of strongly and rapidly driven electrons in the presence of weak scattering by phonons. The power absorbed from the driving field is continuously dissipated by phonon modes, leading to a quasi-equilibrium in the electron distribution. We use the Kronig-Penney model with varying effective mass to establish the growth parameters of an InAs/InP nanowire near optimal for third harmonic generation at terahertz frequency range. © *2015 AIP Publishing LLC*. [http://dx.doi.org/10.1063/1.4921929]

I. INTRODUCTION

When electrons in a crystal band are driven by an external time-independent electric field, they move periodically across the Brillouin zone, creating characteristic Bloch oscillations.[1–5] The frequency of the oscillations, $\omega_B = eEa/\hbar$, where a is the unit cell size, coincides with the energy separation between neighboring states localized on a Wannier-Stark ladder.[5,6] The effect has been observed for electrons/holes in semiconducting superlattices,[7,8] for atoms trapped in a periodic optical potential,[9] and for light propagating in a periodic array of waveguides, with gradient of the temperature or of the refraction index working as an effective electric field.[10–12]

Combining the effects of a strong, time-periodic driving field, with the nonlinearity of the Bloch oscillations leads to higher harmonic generation of the driving frequency.[13–16] This effect has been observed in semiconductor superlattices driven at terahertz frequencies with a free-electron laser,[17] and more recently in bulk ZnO crystals strongly driven by a pulsed infrared laser,[18] and in bulk GaSe crystals driven by short 30 THz pulses.[19] The application of the driving field in short, few-cycle pulses was necessary to ensure that the absorbed energy could be transferred to the lattice and dissipated. Relative importance of intra- and inter-band transitions for higher harmonic generation in these experiments is discussed in Refs. 20 and 21.

Semiconductor superlattices are an ideal system in which to observe these high-field effects. The transport of carriers through these structures can be described in terms of coherent motion through minibands in the energy spectrum.[22] Subsequently, the effects of intense driving fields can be described based on the modification of these minibands.[23] The mechanisms of charge transport in semiconductor superlattices in the presence of strong fields have been extensively studied in terms of miniband transport, Wannier-Stark hopping, and photon-assisted transport.[24,25]

In this work, we suggest that frequency multiplication due to periodically driven Bloch oscillations could also be observed in a steady-state setting, e.g., a periodically modulated nanowire (or an array of such nanowires) continuously driven by high-amplitude terahertz radiation (see Fig. 1). In the weak-scattering limit, the quantum efficiency of frequency tripling for such a system can be as high as 93%. The high efficiency of third harmonic generation presents a novel means of THz radiation and has been previously studied for GaAs superlattices.[26,27]

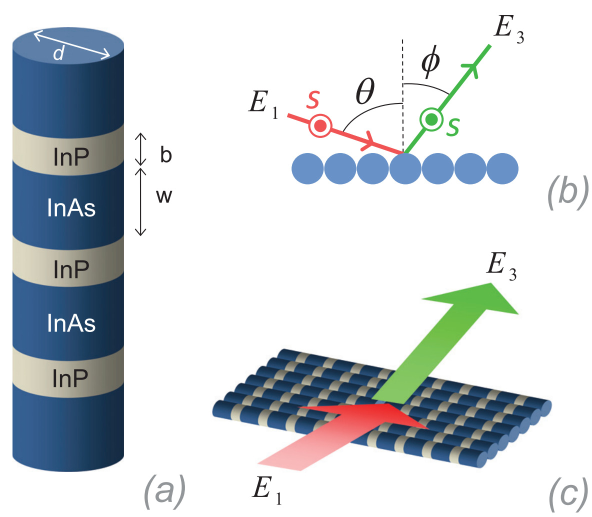

FIG. 1. (a) A nanowire made with alternating InAs/InP regions. (b) and (c) Schematic of the third harmonic generation with a planar array of such nanowires. The driving field is s-polarized so that the electric field E_1 be parallel to the nanowires. The generated third harmonic will have the same polarization but propagate at a different angle.

a)Electronic mail: kathleen.hamilton@email.ucr.edu

For a nanowire in mechanical contact with an insulating, optically transparent substrate, a quasi-equilibrium electron distribution will be reached as the power absorbed from the driving field will be continuously dissipated into phonon modes. This distribution can be quite different from the initial, equilibrium Fermi distribution. In particular, at the driving field amplitude which is optimal for third harmonic generation, the distribution can be both broadened and inverted. The inversion of the distribution occurs once the driving field amplitude exceeds the dynamical localization threshold.[28,29]

Technically, we combine the Floquet quasi-energy description with the Keldysh Green's function technique to obtain the semiclassical master equation for a one-dimensional band of strongly and rapidly driven electrons in the presence of a phonon bath; this equation becomes exact for weak electron-phonon coupling. We solve the master equation numerically to find the electron distribution function at a given driving field frequency (fixed at $\Omega/2\pi = 1$ THz) and the field amplitude chosen to suppress the generation of the principal harmonic. This electron distribution is used as an input for calculating the time-dependent current and the intensity radiated at different harmonics of the driving field frequency. We use these results to find the optimal dimensions of a periodically modulated InAs/InP nanowire, which would yield the most efficient frequency tripling of 1 THz radiation.

II. THEORETICAL APPROACH

We consider a single-band one-dimensional metallic wire driven by a harmonic electric field with the amplitude E_0 and frequency Ω, and coupled to substrate phonons

$$H = H_0 + H_{\text{e–ph}} + H_{\text{ph}}, \tag{1}$$

where the electron, electron-phonon, and phonon Hamiltonians are, respectively,

$$H_0 = \sum_k \varepsilon(k + A(t)) c_k^\dagger c_k, \tag{2}$$

$$H_{\text{e–ph}} = V^{-1/2} \sum_{\mathbf{q},k} M_{\mathbf{q},k} c_{k+q_\parallel}^\dagger c_k (b_\mathbf{q} + b_{-\mathbf{q}}^\dagger), \tag{3}$$

$$H_{\text{ph}} = \sum_\mathbf{q} \omega_\mathbf{q} b_\mathbf{q}^\dagger b_\mathbf{q}. \tag{4}$$

Here, c_k ($c_k^\dagger$) is the annihilation (creation) operator for an electron with one-dimensional momentum $\hbar k$ and energy $\varepsilon(k)$. To apply our results to a periodically modulated nanowire, we assume a tight-binding model with the electronic spectrum

$$\varepsilon(k) = -2J\cos(ka), \tag{5}$$

where J is the hopping matrix element and a is the period of the potential along the chain. The electric field is incorporated into the Hamiltonian through the vector potential of the driving field, $A(t) = A_0 \sin\Omega t$ with $A_0 = eE_0/\hbar\Omega$. Phonon annihilation (creation) operators $b_\mathbf{q}$ and $b_\mathbf{q}^\dagger$ are labeled with the three-dimensional wavevector $\mathbf{q} \equiv (q_\parallel, \mathbf{q}_\perp)$ and $\omega_\mathbf{q}$ is the phonon frequency (electron spin and phonon branch indices are suppressed). The factors $M_{\mathbf{q},k} = \alpha_{\mathbf{q},k}(\hbar/2\omega_\mathbf{q})^{1/2}$ are the matrix elements for electron-phonon scattering.

We ignore the effects of disorder or electron-electron interactions, and consider lattice phonons in thermal equilibrium at temperature $\hbar/(k_B\beta)$. We do not include directly the scattering by phonon modes of the nanowire, assuming that they are strongly hybridized with those of the substrate, with the corresponding effects incorporated in the matrix elements $M_{\mathbf{q},k}$. The electron-phonon coupling is considered to be weak, meaning that the phonon scattering time is long compared to the period $\tau \equiv 2\pi/\Omega$ of the driving field.

In the limit where electron-phonon scattering [Eq. (3)] is suppressed, the electron (quasi)momentum $\hbar k$ is conserved; this requires that electron distribution function f_k be stationary. Weak electron-phonon scattering with the characteristic rates $\Gamma \ll \Omega$ cannot change the distribution function significantly over a single period τ. Instead, in this regime relatively small coherent changes in electrons' density matrix accumulate coherently over many periods. The corresponding effective transition rates $\Gamma_{k,k'}$ [see Eq. (20), below] account for phonon emission/absorption "assisted" by multiple quanta of the driving field. As a result, over time, the initial electron distribution function [e.g., equilibrium at the temperature $\hbar/(k_B\beta)$] will evolve into a stationary non-equilibrium distribution determined by the transition rates $\Gamma_{k,k'}$.

A. Modified energy spectrum of the driven system

The dynamics of the strongly driven electrons with the Hamiltonian (2) is characterized by the phases

$$\varphi_k(t) = \int_0^t dt' \varepsilon(k + A(t')). \tag{6}$$

The phase accumulated over a period, $\varphi_k(\tau)$, can be expressed in terms of the average particle energy with the momentum $\hbar k$

$$\langle \varepsilon_{k+A} \rangle \equiv \tau^{-1} \int_0^\tau dt\, \varepsilon(k + A(t)); \tag{7}$$

clearly, this energy can be also identified as the Floquet energy of a single-electron state. While Eq. (7) does not include the usual additive uncertainty $m\Omega$, this particular choice has the advantage that in the weak-field limit, $A_0 \to 0$, $\langle \varepsilon_{k+A} \rangle$ recovers the zero-field spectrum $\varepsilon(k)$.

The average energy (7) also coincides with that introduced in the theory of dynamical localization.[28,29] Dynamical localization occurs when the effective band becomes flat, i.e., $\langle \varepsilon_{k+A} \rangle \to 0$. The corresponding condition is most easily obtained in the special case of tight-binding model with the spectrum (5)

$$\langle \varepsilon_{k+A} \rangle = -2\tilde{J}\cos(ka), \quad \tilde{J} \equiv J\, J_0(A_0 a), \tag{8}$$

where $J_0(z)$ is the zeroth order Bessel function. With the driving field amplitude increasing from zero the bandwidth is gradually reduced; it switches sign at the roots of the Bessel function, $A_0 a = \zeta_{0n}$. The first time this happens corresponds to the electric field $E_0 = \zeta_{01}\hbar\Omega/ea$, where $\zeta_{01} \approx 2.405$.

B. Frequency multiplication with weak scattering

We obtain the instantaneous current by averaging the canonical velocity operator $\partial H/\partial A$ over the electron distribution function $f_k \equiv \langle c_k^\dagger c_k\rangle$

$$i(t) = C_f(t)\,\sin A(t)a + S_f(t)\,\cos A(t)a, \tag{9}$$

where we assumed the tight-binding spectrum (5) and used the definitions

$$C_f(t) \equiv 2J\int \frac{dk}{2\pi}\cos(ka)f_k, \tag{10}$$

$$S_f(t) \equiv 2J\int \frac{dk}{2\pi}\sin(ka)f_k. \tag{11}$$

In the absence of scattering f_k becomes time independent, and in this limit Eq. (9) is fully consistent with the results of Ref. 13. We consider the limit of weak but non-zero scattering where the Markovian master equation (19) is applicable. Here, the stationary distribution function f_k is also time-independent and always symmetric, $f_{-k} = f_k$. Thus, $S_f(t) = 0$ while $C_f(t) = C_f$ is a time-independent pre-factor. The Fourier components of the current are obtained directly

$$i(t) = 2C_f \sum_{m=1,3,5,\ldots} J_m(A_0 a)\sin(m\Omega t), \tag{12}$$

where the summation is over the odd harmonics m. By choosing $A_0 a = \zeta_{11} \approx 3.8317$, the first harmonic can be fully suppressed, which leaves the third harmonic dominant. The maximal value for the fraction of the energy emitted into the third harmonic (93.34%) is found in close vicinity of this amplitude, see Fig. 2.

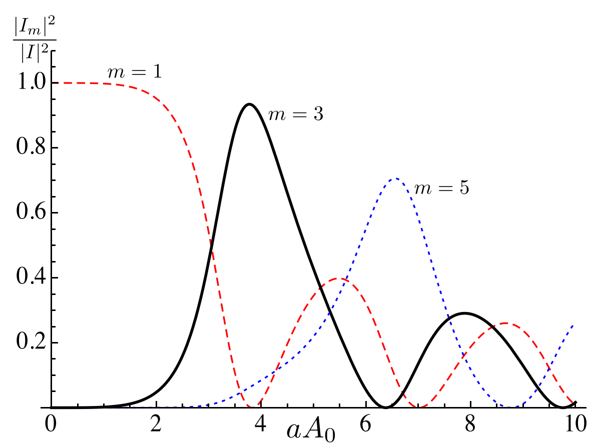

FIG. 2. Normalized magnitude squared of the Fourier harmonics of the instantaneous current, $|I_m|^2$, for $m=1$ (red dashed), $m=3$ (black, solid), and $m=5$ (blue, dotted) plotted as a function of the dimensionless amplitude of the vector potential of the driving field, see Eq. (2). The intensities $|I_m|^2$ correspond to the power emitted in the corresponding harmonics when multiple nanowires are used in a planar geometry, see Figs. 1(b) and 1(c).

C. Transition kinetics in a driven system

We use the Keldysh non-equilibrium Green's function (GF) formalism[30–33] along with a perturbation theory expansion with respect to the entire time-dependent electron Hamiltonian (2); the corresponding evolution is solved exactly in terms of the phases (6). Previously, related approaches have been used in several contexts.[34–40] Here, instead of solving the corresponding equations numerically, we take the limit of weak electron-phonon coupling and analytically derive the semiclassical master equation for electron distribution function averaged over the period of the driving field, see Eqs. (19) and (20). The same master equation can also be derived from the formalism by Konstantinov and Perel'[41] with the help of an appropriate resummation of the perturbation series.[42]

In the interaction representation with respect to the time-dependent Hamiltonian (2), the electron operators acquire time-dependence $e^{-i\varphi_k(t)}c_k$ with quasiperiodic phases (6). We separate these phases by defining the "lower-case" GFs

$$g_k(t_2,t_1) = e^{-i\varphi_k(t_2)}G_k(t_2,t_1)e^{i\varphi_k(t_1)}, \tag{13}$$

where the "upper-case" $G_k(t_2,t_1)$ is any of the conventional GFs introduced in the Keldysh formalism.[30–33] These phases introduce rapid oscillations in the self-energy, making the direct Wigner transformation difficult. We notice, however, that in the limit of weak electron-phonon coupling, the GFs (13) are expected to change only weakly when both time arguments are incremented by the driving period τ. This implies that in the following decomposition:

$$g_k(t_2,t_1) = \sum_m g_{k,m}(t,T)e^{-im\Omega T}, \tag{14}$$

$t \equiv t_2 - t_1$ is the "fast" time, while $T \equiv (t_2+t_1)/2$ is the "slow" time when it appears as an argument of thus defined Floquet components $g_{k,m}(t,T)$ of the GF.[43,44] The Dyson equations for similarly defined lower-case Keldysh $g^K_{k,m}$ and retarded $g^R_{k,m}$ GFs[31] have the form

$$(i\partial_T + m\Omega)g^K_{k,m}(t,T) = I^K_{\rm coll}, \tag{15}$$

$$i\partial_t g^R_{k,m}(t,T) = \delta_{m,0}\,\delta(t) + I^R_{\rm coll}, \tag{16}$$

where $I^K_{\rm coll}$ and $I^R_{\rm coll}$ are the collision integrals originating from the corresponding self-energy functions. The collision integrals being relatively small, both $g^K_{k,m}$ and $g^R_{k,m}$ are dominated by the $m=0$ components.

To derive the semiclassical master equation, we write the equations for the $m=0$ components of the "lesser" $g^<$ and "greater" $g^>$ GFs,[31] perform the Wigner transformation replacing the fast time variable t by the frequency ω, and use a version of the Kadanoff-Baym ansatz[45,46]

$$g^<_{k,0}(\omega,T) = iA_{k,0}(\omega,T)f_k(T). \tag{17}$$

The corresponding spectral function

$$A_{k,0}(\omega,T) = i[g^<_{k,0}(\omega,T) - g^>_{k,0}(\omega,T)] = 2\,\Im{\rm m}g^R_{k,0}(\omega,T), \tag{18}$$

is not solved for self-consistently. We assume a sharply peaked Lorentzian function in order to obtain a phenomenological model of the driven system and define the non-equilibrium electron distribution function $f_k(T)$ from the function $g^<$. The width of the Lorentzian, $\Gamma/2$, is treated as a phenomenological constant and is also not found self-consistently. We assume the doubled width, Γ, to be much smaller than both the bandwidth of the system and the frequency of the driving field, $\Gamma \ll \min(4|\tilde{J}|, \Omega)$.

The use of the Kadanoff-Baym approximation requires us to approximate the scattering as momentum-independent. We also assumed that any electron spectrum renormalization due to electron-phonon coupling has been included in the Hamiltonian (2), and assumed the electron-phonon coupling to be weak.

The resulting master equation for weak electron-phonon interactions has the following standard form:

$$\frac{d}{dt}f_k(T) = \int \frac{dk'}{2\pi}\{\Gamma_{k,k'}\left[1-f_{k'}(T)\right]f_k(T) - \Gamma_{k',k}f_{k'}(T)\left[1-f_k(T)\right]\}, \tag{19}$$

where the transition rates are

$$\Gamma_{k,k'} = 2\sum_m |S_{k,k'}(m)|^2 \int_0^\infty d\omega\, W_{k,k'}(\omega) \times [(n_\omega+1)\delta_\Gamma(\Delta\varepsilon^{(m)}_{k,k'} - \hbar\omega) + n_\omega \delta_\Gamma(\Delta\varepsilon^{(m)}_{k,k'} + \hbar\omega)]. \tag{20}$$

Here, $W_{k,k'}(\omega)$ is the phonon spectral function (density of states weighted by the square of the coupling) for a given momentum $q_\parallel = k' - k$ along the wire, see Eq. (3), $n_\omega \equiv [\exp(\beta\omega) - 1]^{-1}$ is the phonon distribution function, $\delta_\Gamma(\epsilon)$ is the broadened δ-function, a Lorentzian of width Γ, and the energy increment

$$\Delta\varepsilon^{(m)}_{k,k'} \equiv \langle\varepsilon_{k+A}\rangle - \langle\varepsilon_{k'+A}\rangle - m\hbar\Omega, \tag{21}$$

is the energy carried in or out by phonons, depending on its sign. Note that this energy includes m quanta of the driving field, emitted or absorbed, depending on the sign of $m = 0, \pm 1, \ldots$. In Eq. (21), $\langle\varepsilon_{k+A}\rangle$ is the time-average energy of a driven electron, see Eq. (7). The matrix elements $S_{k,k'}(m)$ are the Fourier expansion coefficients of the product of the two phase factors, $e^{i\delta\varphi_k(t) - i\delta\varphi_{k'}(t)}$, where $\delta\varphi_k(t) \equiv \varphi_k(t) - t\langle\varepsilon_{k+A}\rangle$ is the periodic part of the phase. These matrix elements satisfy the sum rule

$$\sum_{m=-\infty}^{\infty} |S_{k,k'}(m)|^2 = 1. \tag{22}$$

Clearly, the equilibrium Fermi distribution for f_k is only obtained in the limit of small electric field amplitudes, such that $S_{k,k'}(m)$ with $m = 0$ gives the dominant contribution.

III. SIMULATION RESULTS

The following results have been obtained by numerically finding the stationary solution of the discretized version of the master equation (19) with transition rates (20), where the standard Kadanoff-Baym approximation was used, $\Gamma \to 0$. A simple model for the phonon spectral function, $W_{k,k'}(\omega) = \gamma^2\theta(\omega - s|k-k'|)$, was used, with the sound speed $s = 5\times 10^3$ m/s as appropriate for typical 3D acoustical phonons. Since we assume no other scattering mechanisms, the quasi-equilibrium distribution functions f_k and other results do not depend on the magnitude of the electron-phonon coupling.

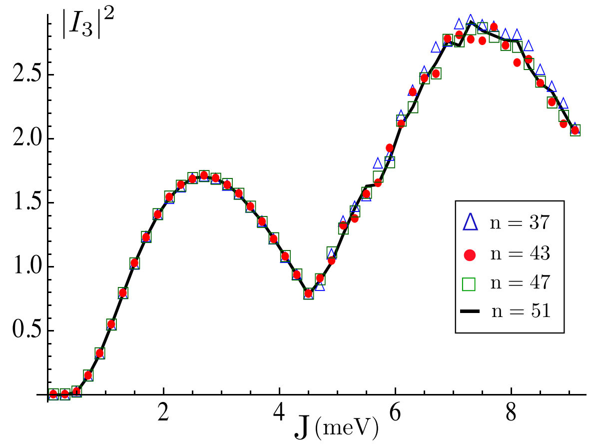

FIG. 3. Magnitude squared of the third harmonic of the instantaneous current (arbitrary units), plotted as a function of the tight-binding parameter J, computed with $N_k = 37$, 43, 47, and 51 discrete momentum points as indicated in the caption. See text for other simulation parameters. The pronounced minima are caused by the flattening of the distribution function near thresholds of m-photon-assisted scattering between the vicinities of $k = 0$ and $k = \pm\pi/a$, with m even.

For simulations, we set the phonon temperature at 4.2 K, the lattice period $a = 8.64$ nm, the average electron filling at 1/2, and choose the driving field frequency $\Omega/2\pi = 10^{12}$ Hz (energy $\hbar\Omega \approx 4.14$ meV). Also, the amplitude $A_0 a = \zeta_{11} \approx 3.8317$ is fixed, which corresponds to the point where the first harmonic generation is fully suppressed [see Fig. 2]. At this point, the effective coupling is $\tilde{J} = J J_0(\zeta_{11}) \approx -0.403 J$, which creates an inverted and somewhat narrowed band. The effective bandwidth is smaller than $\hbar\Omega$ for $J < 2.57$ meV.

In Fig. 3, we show the intensity $|I_3|^2$ of the radiated third harmonic (in arbitrary units) as a function of the tight-binding hopping parameter J. The overall upward trend reflects the linear scaling of the current with J. The plot has a series of pronounced maxima and minima related to the structure of the distribution function f_k, see Fig. 4. Indeed, at the first maximum of the radiated intensity $|I_3|^2$, $J = 2.7$ meV, the distribution function has a well-defined minimum at $k = 0$ and symmetric maxima at $k = \pm\pi/a$ [Fig. 4(b)]; notice the population inversion consistent with negative $\tilde{J}$. On the other hand, the distribution in Fig. 4(c) corresponding to the first minimum of radiated intensity, $J = 4.5$ meV, is much flatter. This flattening can be traced to a sharp increase of the transition rates connecting the regions of momentum space near $k = 0$ and $k = \pi/a$. This is illustrated in Fig. 5, where transition rates between $k = 0$ and $k = \pi/a$ are shown. The corresponding phases $\delta\varphi_{\pi/a} = -\delta\varphi_0$ have only even harmonics $m\Omega$, $m = 2, 4, \ldots$, and

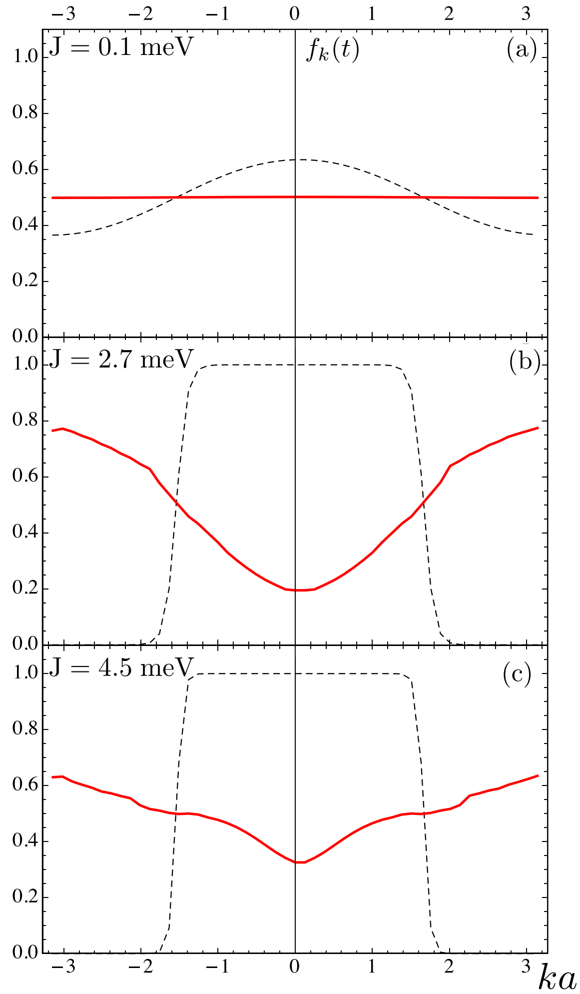

FIG. 4. Solid lines: the stationary distribution functions obtained by solving discretized versions of Eqs. (19) and (20) with $N_k = 51$ momentum points and the tight-binding parameters J as indicated. See text for other simulation parameters. Dashed lines: equilibrium Fermi distribution functions.

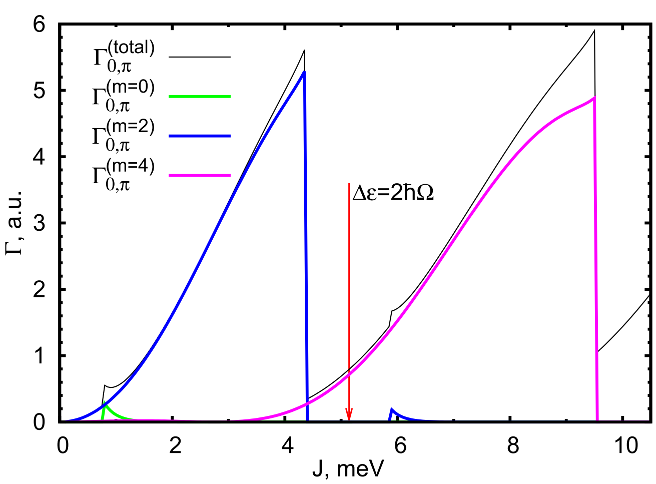

FIG. 5. The transition rate (20) (arbitrary units) for scattering between the sites at $k = -\pi/a$ and $k = 0$ (black, solid) and the individual contributions from m-photon assisted processes as indicated. The vertical arrow at $J = 5.1$ meV indicates the threshold for the $m = 2$ transition, $|4\tilde{J}| = 2\hbar\Omega$; the large peak to the left and the small peak to the right of this point correspond to phonon emission and absorption, respectively.

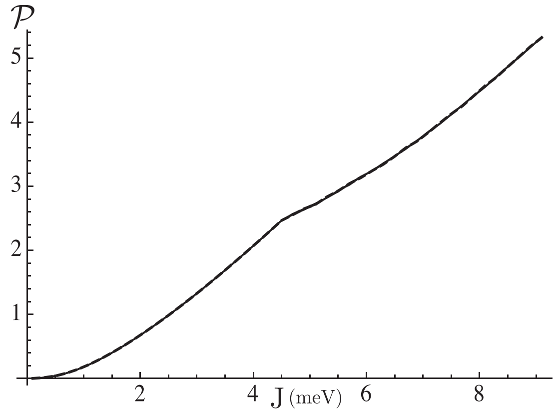

FIG. 6. Scaling of the average power (arbitrary units) dissipated into the phonon modes as a function of the tight-binding parameter J. The four curves on top of each other correspond to the same numbers of discrete momentum points N_k as in Fig. 3.

the threshold values of J for different m correspond to sharp maxima of $\Gamma_{0,\pi/a}$.

We verified that the results remain qualitatively the same when a finite width of the electron spectral function, $\Gamma \leq 1$ meV, is used to calculate the rates in Eq. (20) (data not shown). We also tried using a more general scattering model which includes both acoustical and optical phonons (not shown). In this more general case, the shape of the stationary distribution function f_k depends on the relative strength of the couplings. We find that for an optical mode sufficiently sharp, $\Gamma_{opt} \lesssim 1$ K, and with sufficiently small integrated strengths, the qualitative behavior of the third harmonic also remains unaffected.

In Fig. 6, we show how the average power $\mathcal{P}$ radiated into the phonon modes scales with the tight-binding parameter J. While general dependence on J is monotonic, at $J = 4.5$ meV, where the third harmonic has a minimum, $\mathcal{P}$ changes slope.

IV. PROPOSED EXPERIMENTAL DESIGN

The simulation results in Sec. III suggest that the optimal system for third harmonic generation would be a one-dimensional metallic conductor with an unrenormalized bandwidth close to 2.6 times the energy $\hbar\Omega$ of the driving field quanta (bandwidth of about 11 meV for $\Omega/2\pi = 1$ THz is needed), and a wide gap to reduce the absorption of the generated harmonics. One option to satisfy these requirements is to use modulated semiconductor nanowires. Here, we estimate the growth parameters of an InAs/InP nanowire,[47] which would have a near optimal band structure for generating the third harmonic of a 1 THz driving field.

We calculate the band structure of the modulated nanowire modeling it as a stack of cylinders with isotropic (bulk) electron effective masses $m^*_{\mathrm{InAs}} = 0.073 m_e$ and $m^*_{\mathrm{InP}} = 0.027 m_e$ for the InAs and InP carriers, respectively, as appropriate for the nanowire diameter we used in the calculations.[48] We set the barrier height of $V_0 = 0.636$ eV, found from the four-band model simulations, which is close to experimentally observed[47,49] 0.6 eV. To ensure a relatively large gap, we chose the nanowire diameter $d = 20$ nm

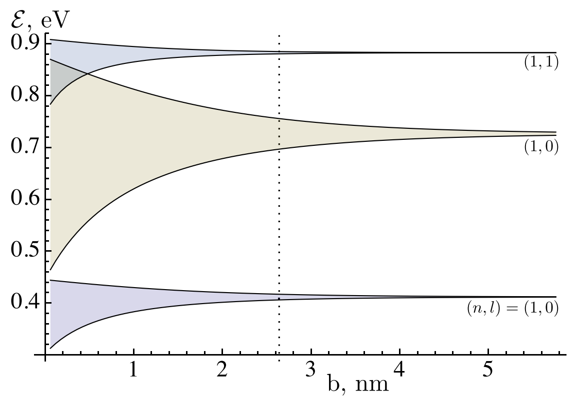

FIG. 7. Energies of the three lowest bands computed using the Kronig-Penney model with effective mass modulation corresponding to an InAs/InP nanowire with diameter $d = 20$ nm, InAs well width $w = 6.0$ nm, plotted as a function of InP barrier width, b. The labels indicate the radial n and angular l quantum numbers of dimensional quantization. The dashed line at $b = 2.64$ nm gives a bandwidth 10.9 meV, or tight-binding parameter $J = 2.7$, corresponding to the first maximum of the third harmonic in Fig. 3.

and InAs well width $w = 6.0$ nm. Separating the radial and angular parts of the corresponding wave functions, we obtained a version of the Kronig-Penney model with effective mass modulation, and effective barrier dependent on the transverse momentum $\hbar\kappa_{nl}$. We plot the first few allowed energy bands as a function of InP barrier width b in Fig. 7.

In particular, we conclude that an InAs/InP nanowire of diameter $d = 20.0$ nm, well width of $w = 6.0$ nm, and barrier width of $b = 2.64$ nm [Fig. 1(a)] would have the lowest band with a width of approximately 10.9 meV. The next band would be separated by a gap of 280 meV [Fig. 7]. These parameters are near optimal for third harmonic generation at $\Omega/2\pi = 1$ THz.

One possible device design could involve depositing of a number of parallel modulated nanowires on a substrate, with an s-polarized driving field incident on the surface at angle θ so that the electric field of the wave be directed along the nanowires [Figs. 1(b) and 1(c)]. Then, both the reflected signal and the first harmonic are going to be propagating at the same reflection angle θ, while the propagation direction of the third harmonic can be found from the Snell's law, $\sin\theta = 3\sin\phi$, which accounts for the wavelengths ratio.

V. SUMMARY

In this work, we suggest a possibility that frequency multiplication due to periodically driven Bloch oscillation may be possible in a quasistationary setting, with the help of a narrow-band one-dimensional conductor. A quasi-equilibrium electron distribution is possible because the energy absorbed from the driving field is continuously dissipated by the bulk phonons.

For a periodically modulated InAs/InP nanowire with the period $a = 8.64$ nm, and the driving field frequency $\Omega/2\pi = 1$ THz, the emission of the first harmonic is suppressed with the dimensionless vector potential amplitude $A_0 a \approx 3.83$, which gives the electric field amplitude $E_0 = \hbar\Omega A_0/e \approx 1.8 \times 10^6$ V/m, corresponding to the energy flux of about 0.5 MWt/cm^2. At this kind of power, many effects could lead to eventual run-away overheating of the system, e.g., direct absorption by the substrate, or even a relatively weak disorder scattering in the nanowire. We hope that a quasi-continuous operation would still be possible, with the driving field pulse duration of a few milliseconds, as opposed to few cycles in the experiments.[18,19]

ACKNOWLEDGMENTS

The authors are grateful to G. Chattopadhyay, K. Cooper, and R. A. Suris for multiple helpful discussions and to C. Pryor for letting us to use his dot code for nanowire calculations. This work was supported in part by the U.S. Army Research Office Grant No. W911NF-11-1-0027 and by the NSF Grant No. 1018935.

[1] F. Bloch, "Über die Quantenmechanik der Elektronen in Kristallgittern," Z. Phys. A **52**, 555–600 (1929).
[2] V. A. Yakovlev, "On the theory governing the conductivity of electrons in the narrow bands of semiconductors in a strong electric field," Sov. Phys.-Solid State **3**, 1442 (1961) [Fiz. Tv. Tela **III**, 1983 (1961)].
[3] V. A. Yakovlev, "Light absorption by electrons of nonmetallic crystals in an electric field," Sov. Phys. JETP-USSR **13**, 1194 (1961) [JETP **40**, 1695 (1961)].
[4] L. V. Keldysh, "Optical characteristics of electrons with a band energy spectrum in a strong electric field," Sov. Phys. JETP-USSR **16**, 471 (1963) [JETP **43**, 661 (1962)].
[5] G. H. Wannier, "Dynamics of band electrons in electric and magnetic fields," Rev. Mod. Phys. **34**, 645–655 (1962).
[6] H. Fukuyama, R. A. Bari, and H. C. Fogedby, "Tightly bound electrons in a uniform electric field," Phys. Rev. B **8**, 5579–5586 (1973).
[7] C. Waschke, H. G. Roskos, R. Schwedler, K. Leo, H. Kurz, and K. Köhler, "Coherent submillimeter-wave emission from Bloch oscillations in a semiconductor superlattice," Phys. Rev. Lett. **70**, 3319–3322 (1993).
[8] E. E. Mendez and G. Bastard, "Wannier-stark ladders and Bloch oscillations in superlattices," Phys. Today **46**(6), 34 (1993).
[9] M. Ben Dahan, E. Peik, J. Reichel, Y. Castin, and C. Salomon, "Bloch oscillations of atoms in an optical potential," Phys. Rev. Lett. **76**, 4508–4511 (1996).
[10] T. Pertsch, P. Dannberg, W. Elflein, A. Bräuer, and F. Lederer, "Optical Bloch oscillations in temperature tuned waveguide arrays," Phys. Rev. Lett. **83**, 4752–4755 (1999).
[11] R. Morandotti, U. Peschel, J. S. Aitchison, H. S. Eisenberg, and Y. Silberberg, "Experimental observation of linear and nonlinear optical Bloch oscillations," Phys. Rev. Lett. **83**, 4756–4759 (1999).
[12] D. N. Christodoulides, F. Lederer, and Y. Silberberg, "Discretizing light behaviour in linear and nonlinear waveguide lattices," Nature **424**, 817–823 (2003).
[13] K. A. Pronin, A. D. Bandrauk, and A. A. Ovchinnikov, "Harmonic generation by a one-dimensional conductor: Exact results," Phys. Rev. B **50**, 3473–3476 (1994).
[14] F. H. M. Faisal and J. Z. Kamiński, "Floquet-Bloch theory of high-harmonic generation in periodic structures," Phys. Rev. A **56**, 748–762 (1997).
[15] A. K. Gupta, O. E. Alon, and N. Moiseyev, "Generation and control of high-order harmonics by the interaction of an infrared laser with a thin graphite layer," Phys. Rev. B **68**, 205101 (2003).
[16] D. Golde, T. Meier, and S. W. Koch, "High harmonics generated in semiconductor nanostructures by the coupled dynamics of optical inter- and intraband excitations," Phys. Rev. B **77**, 075330 (2008).
[17] M. C. Wanke, J. S. Scott, S. J. Allen, K. D. Maranowski, and A. C. Gossard, "Terahertz harmonic generation from Bloch-oscillating superlattices in quasi-optical arrays," Proc. SPIE **3617**, 148–158 (1999).
[18] S. Ghimire, A. D. DiChiara, E. Sistrunk, P. Agostini, L. F. DiMauro, and D. A. Reis, "Observation of high-order harmonic generation in a bulk crystal," Nat. Phys. **7**, 138–141 (2011).
[19] O. Schubert, M. Hohenleutner, F. Langer, B. Urbanek, C. Lange, U. Huttner, D. Golde, T. Meier, M. Kira, S. W. Koch, and R. Huber, "Sub-cycle control of terahertz high-harmonic generation by dynamical Bloch oscillations," Nat. Photonics **8**, 119–123 (2014).

[20]P. G. Hawkins and M. Y. Ivanov, "Role of subcycle transition dynamics in high-order-harmonic generation in periodic structures," Phys. Rev. A **87**, 063842 (2013).
[21]G. Vampa, C. R. McDonald, G. Orlando, D. D. Klug, P. B. Corkum, and T. Brabec, "Theoretical analysis of high-harmonic generation in solids," Phys. Rev. Lett. **113**, 073901 (2014).
[22]L. Esaki and R. Tsu, "Superlattice and negative differential conductivity in semiconductors," IBM J. Res. Dev. **14**, 61–65 (1970).
[23]M. Holthaus, "Collapse of minibands in far-infrared irradiated superlattices," Phys. Rev. Lett. **69**, 351–354 (1992).
[24]A. Wacker, "Semiconductor superlattices: a model system for nonlinear transport," Phys. Rep. **357**, 1–111 (2002).
[25]G. Platero and R. Aguado, "Photon-assisted transport in semiconductor nanostructures," Phys. Rep. **395**, 1–157 (2004).
[26]M. C. Wanke, A. G. Markelz, K. Unterrainer, S. J. Allen, and R. Bhatt, "Third harmonic generation in a GaAs/AIGaAs superlattice in the Bloch oscillator regime," in *Hot Carriers in Semiconductors*, edited by K. Hess, J.-P. Leburton, and U. Ravaioli (Plenum Press, New York, 1996), p. 135, in Proceedings of the Ninth International Conference on Hot Carriers in Semiconductors, held July 31—August 4, 1995, in Chicago, Illinois.
[27]X. L. Lei, "Current suppression and harmonic generation by intense terahertz fields in semiconductor superlattices," J. Appl. Phys. **82**, 718–721 (1997).
[28]D. H. Dunlap and V. M. Kenkre, "Dynamic localization of a charged particle moving under the influence of an electric field," Phys. Rev. B **34**, 3625–3633 (1986).
[29]F. Grossmann, T. Dittrich, P. Jung, and P. Hänggi, "Coherent destruction of tunneling," Phys. Rev. Lett. **67**, 516–519 (1991).
[30]L. V. Keldysh, "Diagram technique for non-equilibrium processes," Zh. Eksp. Teor. Fiz. **47**, 1515 (1964) [Sov. Phys. JETP **20**, 1018 (1965)].
[31]J. Rammer and H. Smith, "Quantum field-theoretical methods in transport theory of metals," Rev. Mod. Phys. **58**, 323–359 (1986).
[32]A. Kamenev, "Many-body theory of non-equilibrium systems," e-print arXiv:cond-mat/0412296 (2004).
[33]H. Haug and A.-P. Jauho, *Quantum Kinetics in Transport and Optics of Semiconductors*, 2nd ed. (Springer, New York, 2008).
[34]P. L. DeVries, "Calculation of harmonic generation during the multiphoton ionization of the hydrogen atom," J. Opt. Soc. Am. B **7**, 517–520 (1990).
[35]G. Meinert, L. Bányai, P. Gartner, and H. Haug, "Theory of THz emission from optically excited semiconductors in crossed electric and magnetic fields," Phys. Rev. B **62**, 5003–5009 (2000).
[36]R.-B. Liu and B.-F. Zhu, "Nonlinear optics of semiconductors under an intense terahertz field," Phys. Rev. B **68**, 195206 (2003).
[37]J. H. Jiang and M. W. Wu, "Spin relaxation in an InAs quantum dot in the presence of terahertz driving fields," Phys. Rev. B **75**, 035307 (2007).
[38]N. Tsuji, T. Oka, and H. Aoki, "Correlated electron systems periodically driven out of equilibrium: Floquet + DMFTformalism," Phys. Rev. B **78**, 235124 (2008).
[39]C. J. Joachain, N. J. Kylstra, and R. M. Potvliege, *Atoms in Intense Laser Fields* (Cambridge University Press, Cambridge, UK, 2011).
[40]A. F. Kemper, B. Moritz, J. K. Freericks, and T. P. Devereaux, "Theoretical description of high-order harmonic generation in solids," New J. Phys. **15**, 023003 (2013).
[41]O. V. Konstantinov and V. I. Perel, "A graphical technique for computation of kinetic quantities," Zh. Exp. Teor. Fiz. **39**, 197–208 (1960).
[42]L. P. Pryadko and P. Sengupta, "Quantum kinetics of an open system in the presence of periodic refocusing fields," Phys. Rev. B **73**, 085321 (2006).
[43]K. B. Nordstrom, K. Johnsen, S. J. Allen, A.-P. Jauho, B. Birnir, J. Kono, T. Noda, H. Akiyama, and H. Sakaki, "Excitonic dynamical Franz-Keldysh effect," Phys. Rev. Lett. **81**, 457–460 (1998).
[44]K. Johnsen and A.-P. Jauho, "Quasienergy spectroscopy of excitons," Phys. Rev. Lett. **83**, 1207–1210 (1999).
[45]L. P. Kadanoff and G. Baym, *Quantum Statistical Mechanics* (Benjamin, New York, 1962).
[46]P. Lipavský, V. Špička, and B. Velický, "Generalized Kadanoff-Baym ansatz for deriving quantum transport equations," Phys. Rev. B **34**, 6933–6942 (1986).
[47]M. T. Bjork, B. J. Ohlsson, T. Sass, A. I. Persson, C. Thelander, M. H. Magnusson, K. Deppert, L. R. Wallenberg, and L. Samuelson, "One-dimensional heterostructures in semiconductor nanowhiskers," Appl. Phys. Lett. **80**, 1058–1060 (2002).
[48]M. D. Moreira, P. Venezuela, and R. H. Miwa, "InP and InAs nanowires hetero- and homojunctions: Energetic stability and electronic properties," Nanotechnology **21**, 285204 (2010).
[49]C. Thelander, M. T. Björk, M. W. Larsson, A. E. Hansen, L. R. Wallenberg, and L. Samuelson, "Electron transport in InAs nanowires and heterostructure nanowire devices," Solid State Commun. **131**, 573–579 (2004).